Natural convective flow and heat transfer on unconfined isothermal zigzag-shaped ribbed vertical surfaces

Hærvig, Jakob; Sørensen, Henrik

Published in:
International Communications in Heat and Mass Transfer

DOI (link to publication from Publisher):
10.1016/j.icheatmasstransfer.2020.104982

Publication date:
2020

Document Version
Accepted author manuscript, peer reviewed version

Natural convective flow and heat transfer on unconfined isothermal zigzag-shaped ribbed vertical surfaces

J. Hærvig[a], H. Sørensen[a]

[a] *Aalborg University, Department of Energy Technology, Pontoppidanstræde 111, DK-9220 Aalborg, Denmark*

Abstract

Natural convective heat transfer is commonly used as heat transfer mechanism in applications with low heat flux due to its reliability and cost effectiveness. In this study, we introduce zigzag-shaped ribs to vertical, isothermal, heated surfaces with the purpose of increasing natural convective heat transfer. The ribs are characterised by a rib height h, rib length p and vertical pitch distance L. We perform numerical simulations using the Boussinesq approximation by prescribing a linear density-temperature relation and investigate how changes in rib length p/L, rib height h/L affect heat transfer at $\mathrm{Gr_L} = 10^5$ and $\mathrm{Gr_L} = 10^6$ at $\mathrm{Pr} = 0.71$.

The results show how geometric variations affect heat transfer locally. Generally, local heat transfer increases along each outward-facing section and peaks at the tip of each rib. In the limiting case when surface approaches a forward facing step (e.g. $p/L = 1$), a significant decrease in heat transfer is observed on the horizontal section.

A peak in heat transfer is observed for geometries with high rib lengths $p/L = 0.9$, where the surface-averaged Nusselt number is increased by 4.43% compared to the flat surface. This increases to 11.60% when correcting for the increase in surface area.

Keywords: Heat transfer, Natural convection, Zigzag shaped surface, Laminar flow, Geometric variations, Isothermal surface

1. Introduction

Natural convection as heat transfer mechanism has many uses because of its simplicity and lack of additional components such as fan or pump, which ensures reliable operation over extended periods. Even though much research has been devoted to mixed convection [1–3], relatively few studies focus solely on enhancing natural convection by geometrical changes in surface geometry. Therefore further studies on pure natural convection are essential for critical applications where the added maintenance and risk of failure associated with a fan or pump is crucial. Commonly, heat sinks that utilise natural convection are designed with multiple straight simple fins with the purpose of increasing the overall surface area and therefore heat transfer rate. Relatively few studies focus on how surface alterations and if such alterations actually the increase heat transfer rate remain relatively scarce. In some circumstances, such as faces of buildings and electronic circuit boards, surface protrusions exist naturally. In other applications such as heat sinks, there are opportunities to alter surface geometries for higher heat transfer rates. In either case a better understanding of surface alterations affect natural convective heat transfer is therefore important.

Email address: jah@et.aau.dk (J. Hærvig)

Park and Bergles [4], Joshi et al. [5] investigated experimentally how heat-generating protrusions of various size on vertical surfaces affect heat transfer characteristics. Bhavnani and Bergles [6] used a Mach-Zehnder interferometer (MZI) to experimentally investigate natural convective heat transfer from isothermal square ribs and steps on surfaces. Generally, square ribs were shown to decrease heat transfer when compared to a plain vertical surface, which was attributed the presence of stagnation zones just up- and downstream the ribs, which result in a thickening of the thermal boundary layer. Instead, an outward step-like surface with a series of vertical segments was introduced that successfully increased heat transfer.

To decrease stagnation zones up- and downstream the ribs, Bhavnani and Bergles [6], Aydin [7], Tanda [8] suggest adding non-conductive square ribs to the heated surface. In general, studies agree that stagnation zones can be reduced in size but disagree on its effect on heat transfer. While Bhavnani and Bergles [6] report surface-averaged heat transfer enhancements up to 5%, the study by Tanda [8, 9, 10] suggests that only local enhancements in heat transfer can be obtained. As a result adding square ribs to surfaces are commonly reported to decrease heat transfer [11]. In all instances, the spacing between successive ribs should be chosen carefully to ensure that the inter-rib region with enhanced heat transfer is not offset by the inherent stagnation zones.

Dating back to the study by Yao [12], a number of studies on natural convection on vertical wavy surfaces have been published. Moulic and Yao [13, 14] did numerical simulations for wavy surface subject to a constant heat flux and found an overall decrease heat transfer compared to a smooth vertical surface. Molla et al. [15], Molla and Hossain [16] investigated both simple and more complex wavy surfaces with an additional harmonic. By varying both the wave amplitude of the fundamental wave and the harmonic, the study concludes that the heat transfer is more sensitive to the amplitude of the harmonic than the fundamental wave. In general the study by Yao [17] suggests the average Nusselt number to be lower for wavy surfaces than for vertical plane surfaces. However, when correcting for the increment in surface area, heat transfer rate is almost doubled compared to a vertical plane surface.

The transition to turbulence in natural convective flows may significantly change heat transferred. The studies by Sharma et al. [18], Cimarelli and Angeli [19] and Qiao et al. [20] all focus on the route to turbulence and map the transition thoroughly but limit their studies to bare channels without surface alterations. However, as outlined by both Bhavnani and Bergles [21] and Yao [17] the presence of ribs may trigger the transition to turbulence to occur at lower Rayleigh numbers.

As previous studies suggest, the stagnation zones being formed just up- and downstream ribs reduce local heat transfer. In the present study, we study zigzag-shaped surfaces (see figure 1), which have rib angles that are different from 90°. As shown later, these zigzag shaped ribs changes how the flow separates and reattaches to the surface. Starting from a vertical plane surface, we show how different surface perturbations affect the buoyancy-driven flow and local heat transfer. It is worth noting that in the limit of $p/L = 1$, the geometry reduces to the forward-facing step documented by Hærvig et al. [22].

2. Numerical details

2.1. Governing equations and computational domain

We limit our study to cases where $\beta(T_\mathrm{s} - T_\infty) \ll 1$ so that the Boussinesq approximation is valid and temperature variations only affect the governing equations through the gravity term in the y-momentum equation. In general, density-temperature relations can be described by a series of n terms:

$$\frac{\Delta\rho}{\rho_0} = \sum_{i=1}^{n} \beta_i (T - T_\infty)^i \tag{1}$$

where ρ_0 refers to the density at the reference temperature T_∞. In this study a linear density-temperature relation (LDT) is assumed throughout the entire temperature range so that eq. (1) simply reduces to $\Delta\rho/\rho_0 = \beta(T_\infty - T)$. Consequently, we treat the

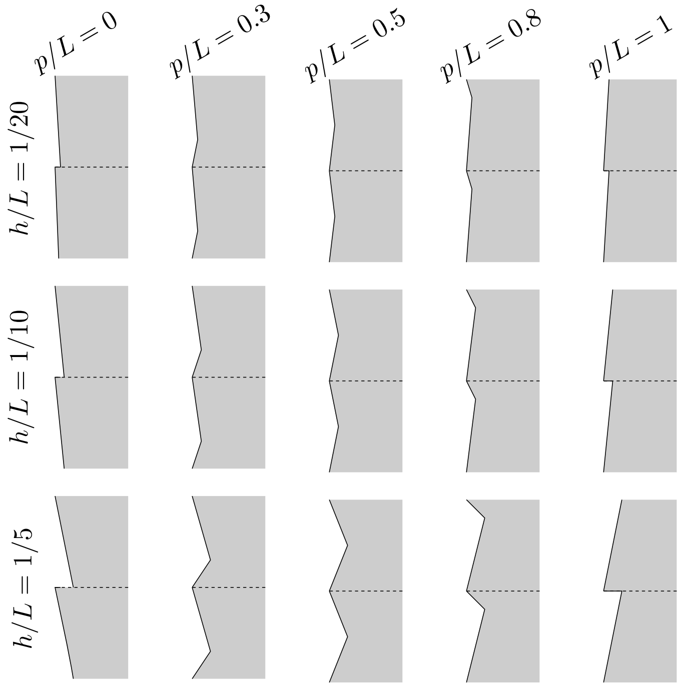

Figure 1: Examples of zigzag ribbed surfaces (two successive ribs shown) with increasing local rib length p/L from left to right and increasing rib height h/L from top to bottom.

temperature T as a passive scalar and solve the time-dependent, incompressible continuity, momentum and temperature equations for buoyant flow:

$$\nabla \cdot \boldsymbol{u} = 0 \tag{2}$$

$$\frac{\partial \boldsymbol{u}}{\partial t} + (\boldsymbol{u} \cdot \nabla)\, \boldsymbol{u} = -\frac{1}{\rho}\nabla p + \nu \nabla^2 \boldsymbol{u} + \boldsymbol{g}\beta\,(T - T_\infty) \tag{3}$$

$$\frac{\partial T}{\partial t} + \boldsymbol{u} \cdot \nabla T = \frac{\nu}{\mathrm{Pr}} \nabla^2 T \tag{4}$$

where $\boldsymbol{g}$ is the gravity vector. The governing equations are discretised using the finite volume method and the second-order accurate Crank-Nicolson scheme is applied for temporal discretisation while second-order accurate central differencing is applied for spatial discretisation. The coupling between velocity and pressure is handled using the Pressure-Implicit with Splitting of Operators (PISO) algorithm [23] with the time step size dynamically being adjusted to ensure a maximum cell convective Courant number Co ≈ 1. Simulations are carried out using OpenFOAM 6 using a custom-built version of the buoyantBoussinesqPimpleFoam solver.

Figure 2 gives an overview of the computational domain along with boundary conditions. In general, the boundary conditions shown in the figure are carefully chosen to ensure the buoyant flow being generated resembles that for truly unconfined surfaces. The zigzag-shaped ribbed surface is prescribed a constant wall temperature T_s. Below the heated wall, an adiabatic wall section ($\partial T/\partial n = 0$) with length $2L$ is added to ensure the boundary layer development on the heated section remains unaffected by the presence of domain boundaries. For the same reason, an additional heated section with surface temperature T_{s} is added above the heated wall of interest.

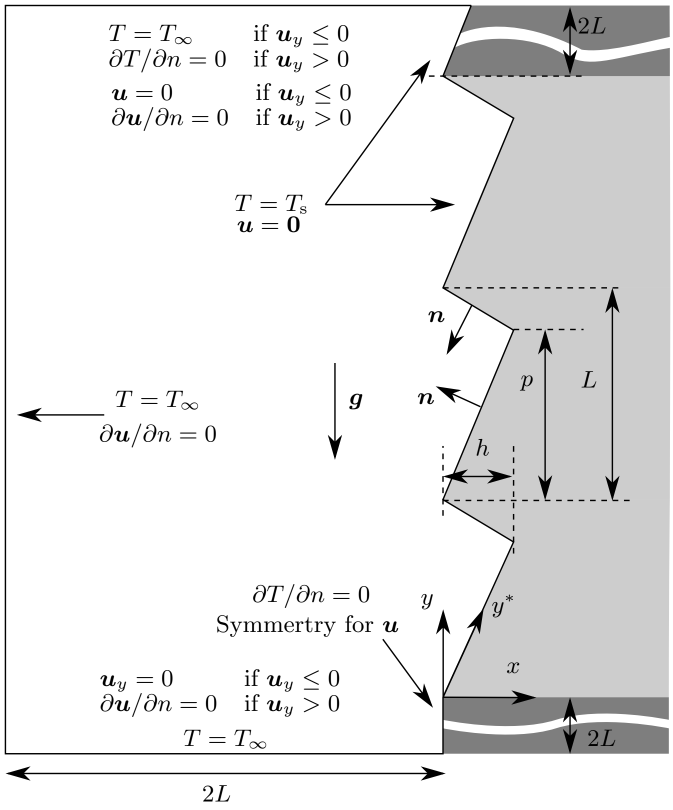

Figure 2: Overview of the geometry, computational domain and boundary conditions. Results are reported for the wall section coloured in light grey. The ribbed wall section is characterised by pitch distance L, local rib length p and rib height h. Furthermore, a local coordinate y^* is defined along the surface so that $y^* = L^* = \sqrt{p^2 + h^2} + \sqrt{(L-p)^2 + h^2}$ at $y = L$.

2.2. Non-dimensionalisation

For buoyancy driven flows with linear density-temperature relations, the problem is solely governed by the Grashof and Prandtl numbers:

$$\mathrm{Gr_L} = \frac{g\beta\,(T_{\mathrm{s}} - T_\infty)\,L^3}{\nu^2} \tag{5}$$

$$\mathrm{Pr} = \frac{\nu}{\alpha} \tag{6}$$

where β is the thermal expansion coefficient, T_{s} is surface temperature, T_∞ is the fluid temperature unaffected by the presence of the wall and L is the vertical pitch distance between two successive ribs. For a plane wall we instead use the vertical coordinate y as reference length:

$$\mathrm{Gr_y} = \frac{g\beta\,(T_{\mathrm{s}} - T_\infty)\,y^3}{\nu^2} \tag{7}$$

Each rib is further geometrically characterised by a local rib length p and rib height h (see figure 2) forming the non-dimensional local rib length p/L and rib height h/L. Local heat transfer along the heated surface is reported by the local Nusselt number:

$$\mathrm{Nu_L} = \frac{\partial T}{\partial n}\frac{L}{T_{\mathrm{s}} - T_\infty} \tag{8}$$

where $\partial T/\partial n$ denotes the local wall normal temperature gradient evaluated at the surface. For a plane wall it is convenient to use the vertical coordinate as reference length:

$$\mathrm{Nu_y} = \frac{\partial T}{\partial n}\frac{y}{T_{\mathrm{s}} - T_\infty} \tag{9}$$

To compare different surface geometries in terms of their enhancement of heat transfer mechanism, the surface-averaged Nusselt number used. This is defined as follows:

$$\overline{\mathrm{Nu}}_{\mathrm{L}} = \frac{\int_A \mathrm{Nu_L}\,\mathrm{d}A}{\int_A \mathrm{d}A} \tag{10}$$

Heat transfer from ribbed surfaces can be increased by either changing the flow field and Consequently the temperature gradient at the surface or by increasing the surface area. To compare the surface geometries account for both factors when comparing the surface geometries, Nusselt numbers based on projected surface length are compared as well. The surface-averaged Nusselt number corrected to account for the increase is surface area $\overline{\mathrm{Nu}}_{\mathrm{L,c}}$ is related to the surface-averaged Nusselt number $\overline{\mathrm{Nu}}_{\mathrm{L}}$ by:

$$\overline{\mathrm{Nu}}_{\mathrm{L,c}} = \overline{\mathrm{Nu}}_{\mathrm{L}}\frac{A}{A_{\mathrm{p}}} \tag{11}$$

where the actual surface area A is larger than the projected surface area A_{p} except for the plane wall where $A = A_p$.

3. Grid and time dependence analysis

To ensure the choice of boundary conditions resembles a truly unconfined flow and to quantify the effect of discretisation error, two measures are taken. First, the numerical code is verified by comparing local heat transfer on a vertical plate to the analytical solution by Ostrach [24] and Fevre [25]. Next, the dependency of grid resolution is examined for a ribbed surface. For a vertical plane wall the analytical solution by Ostrach [24] is given by:

$$\mathrm{Nu_y} = \left(\frac{\mathrm{Gr_y}}{4}\right)^{1/4} g(\mathrm{Pr}) \tag{12}$$

with the fit for $g(\mathrm{Pr})$ proposed by Fevre [25] to account for variations in Prandtl number:

$$g(\mathrm{Pr}) = \frac{0.75\mathrm{Pr}^{1/2}}{\left(0.609 + 1.221\mathrm{Pr}^{1/2} + 1.238\mathrm{Pr}\right)^{1/4}} \tag{13}$$

Figure 3 shows how the numerical simulation from the present study compares to the semi-analytical solution and

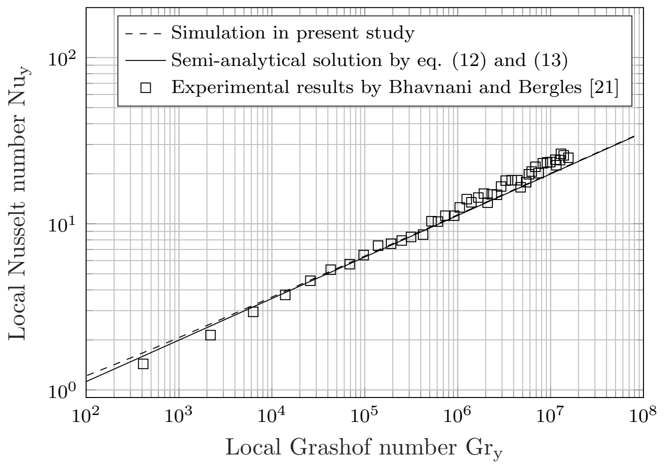

Figure 3: Numerical prediction of local Nusselt number $\mathrm{Nu_y}$ as function of local Grashof number $\mathrm{Gr_y}$ at $\mathrm{Pr} = 0.71$ compared to the semi-analytical solution by Ostrach [24] and Fevre [25] (eq. (12) and (13) respectively) and the experiments by Bhavnani and Bergles [21].

the experiment by Bhavnani and Bergles [21]. As figure 3 shows, the numerical results deviate slightly from the semi-analytical solution at lower Grashof numbers. This can be explained by heat diffusing upstream the heated section, which is not accounted for in the semi-analytical solution. As opposed to the semi-analytical solution, which assumes no heat diffuses upstream the heated plate, the simulations are carried out in a domain that extends a distance of $2L$ upstream the heated plate, which is found to be sufficient to make the results independent of domain size. As the flow develops along the heated plate, the local Nusselt number asymptotically approaches the semi-analytical solution, and at $\mathrm{Gr_y} = 10^8$ the deviation from the semi-analytical solution is a mere 0.6%. To estimate the exact solution for an infinite fine mesh, Richardson extrapolation and the Grid Convergence Index (GCI) are used as suggested by Roache [26]. Using the GCI approach, an error band quantifying the uncertainty in the estimated exact value is obtained. This error band is given by $\mathrm{Nu_{L,e}} \pm \mathrm{Nu_{L,e}}\mathrm{GCI}_{12}$, where subscript e denotes the estimated exact value and GCI_{12} denotes the GCI value obtained from the two finest meshes obtained from:

$$\mathrm{GCI} = \frac{F_\mathrm{s}|\epsilon|}{r^p - 1} \tag{14}$$

where F_s is a safety factor commonly chosen to be be 1.25 as suggested by Roache [26], ϵ is the relative error between the two grids, r is the refinement ratio and p is the order of convergence. Figure 4 shows the sensitivity of grid resolution on the surface-averaged Nusselt number along with the extrapolated value for an infinite fine mesh. The figure shows that asymptotic behaviour is observed for grids with more than 141 cells along the surface of a rib. Furthermore, the figure suggests the grid with 141 cells to be within the error band while the surface-averaged Nusselt number deviates 0.3% from the extrapolated exact value For this mesh, the wall-adjacent cells are placed at

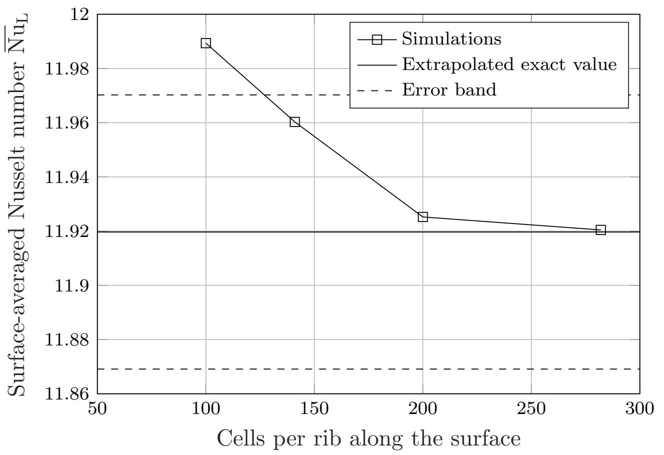

Figure 4: Sensitivity of changes in grid resolution on the surface-averaged Nusselt number $\overline{\mathrm{Nu}}_\mathrm{L}$ for $\mathrm{Gr_L} = 10^6$ and $\mathrm{Pr} = 0.71$ on a ribbed surface with $p/L = 0.8$ and $h/L = 1/5$. The error band is based on a safety factor $F_\mathrm{s} = 1.25$.

$2.5 \cdot 10^{-3}/L$ and successive cell layers grow with 2.5% in the direction perpendicular to the the wall.

Furthermore, as pointed out in previous studies by Bhavnani and Bergles [21] and Yao [17], ribbed surfaces may trigger the transition to turbulence to occur at a lower Grashof number. As such all simulations in the present study are run as transient to resolve any transient phenomenon in the flow. Figure 5 shows a typical example of time convergence of the surface-averaged Nusselt number. As figure 5 shows, the simulation converges

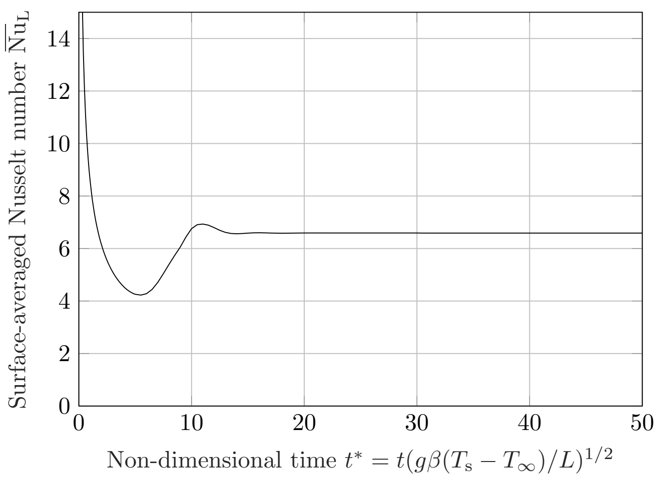

Figure 5: Time-history of the surface-averaged Nusselt number $\overline{\mathrm{Nu}}_\mathrm{L}$ for $\mathrm{Gr_L} = 10^5$, $\mathrm{Pr} = 0.71$ with rib length $p/L = 0.8$ and rib height $h/L = 1/8$.

towards a steady solution where no transients are observed in the flow field. In the remainder of this study, only time-converged results are reported. Furthermore, a domain independence analysis is carried out to ensure that the width of the domain being $2L$ is sufficient to make the results independent of the domain size.

4. Results and discussion

In this section results are presented. First, our discussion is focused on how geometric variations affect the flow and temperature fields and consequently the local Nusselt number along the ribbed surfaces. Next, the surface-averaged Nusselt numbers are compared for the different surfaces and compared to the flat vertical surface, which is used as reference geometry.

4.1. Variations in rib length

Figure 6 shows how streamlines (subfigure 1-4) and the temperature fields (subfigure 5-8) are affected when the rib length p/L is varied between 0.3, 0.6, 0.9 and 1.0. Figure 7 shows the corresponding local Nusselt numbers as function of vertical coordinate y/L. For all rib lengths a local decrease in heat transfer is observed at the innermost points located at $y/L = p/L$, $y/L = 1 + p/L$ and $y/L = 2 + p/L$ explained by a thickening of the thermal boundary layer in these regions. As the figure shows, higher values of p/L cause this effect to become increasingly more pronounced. In the limit of $p/L = 1.0$, corresponding to a forward facing step similar to the one investigated by Hærvig et al. [22], the horizontal section causes the stagnation zone at the innermost point to significantly increase in size. After the innermost point at $y/L = p/L$ (e.g. the outward-facing sections), local heat transfer is increased compared to the plane vertical surface. In all cases local heat transfer peaks at the rib tip, due to a significant thinning of the thermal boundary layer. This is also evident from subfigure 4-6 in figure 6, which shows the temperature fields. Again, this effect is more pronounced for higher p/L-ratios. For all p/L-ratios investigated, local heat transfer peaks at the rib tips. After the rib tip, local heat transfer again attains values below the plane vertical surface. The drop in local heat transfer right after the rib tip is more pronounced for higher rib lengths and the least pronounced for low rib lengths. One exception is the limiting rib with $p/L = 1$, which experiences a more significant drop in heat transfer at the innermost point. Figure 8 gives an overview of the local heat transfer using surface coordinates y^* instead of vertical coordinates y. As shown in figure 8 for the surface with $p/L = 1$, the local Nusselt number is lowest at the innermost points and increases on horizontal section towards the rib tip where the highest heat transfer is observed.

4.2. Variations in rib height

Next, the variations in rib height are introduced for a constant rib length. Figure 9 shows how stream lines (subfigure 1-4) and temperature fields (subfigure 5-8) are affected by variations in rib height from $h/L = 1/32$ to $h/L = 1/8$. Subfigure 1-4 in figure 9 show how streamlines are affected by variations in rib height. As the rib height increases from $h/L = 1/32$ to $h/L = 1/8$, the low velocity stagnation regions at the innermost point and just downstream the rib tip increase in size. This is evident from subfigure 4-6, which shows a thickening of the thermal boundary layer and in turn yields lower local heat transfer rate in this region. Figure 10 shows the effect on the local heat transfer of altering the rib height for a fixed rib length. As seen in the figure, local heat transfer decreases in the region around the innermost point (in this case $y^*/L^* \approx 0.8$) and just downstream the rib tip for higher rib heights. On the outward-facing section between $y^*/L^* \approx 0.8$ and $y^*/L^* = 1.0$, local heat transfer is significantly increased compared to the vertical plate. This effect is again increasingly more pronounced for higher rib heights. Downstream the rib tip, we again observe a local decrease in local heat transfer caused by a stagnation region. After a certain distance downstream the rib tip, the boundary layer again reattaches to the surface and the local heat transfer rate increases.

4.3. Variation in Grashof number

The Grashof number is varied to investigate the relative importance of buoyancy and viscous forces when introduction zigzag-shaped ribs. Two Grashof numbers of 10^5 and 10^6 are simulated, which both represent typical values used for cooling applications. Figure 11 shows how changes in rib length affect the local Nusselt number along the surface. The tendency for the local Nusselt number obtained along the ribbed surface for a higher Grashof number of $\mathrm{Gr_L} = 10^6$ is similar to that obtained for $\mathrm{Gr_L} = 10^5$. Again, stagnation regions are present at the innermost points on the rib surface resulting in a decrease in local heat transfer. On the outward-facing section and at the rib tip, local heat transfer is significantly increased compared to the flat vertical plate. Heat transfer in the region downstream the rib tip is again dominated by stagnation region causing a decrease in local heat transfer. However, for $\mathrm{Gr_L} = 10^6$ compared to $\mathrm{Gr_L} = 10^5$, we observe an increase in local heat transfer at the location where the flow reattaches to the surface. This effect is even more pronounced after the second rib tip around $y^*/L^* \approx 2.4$, where the surface with $p/L = 0.9$ shows an increase of approximately 11% compared to the flat vertical plate.

4.4. Surface-averaged heat transfer

Surface-averaged Nusselt numbers are compared for the different geometric variations. All the numbers are listed in table A.1 in Appendix A. Figure 12 gives an overview of the results in terms of relative difference compared to the flat vertical surface. As shown in the figure, only small enhancements in surface-averaged Nusselt number are generally obtained for the different geometries. As expected, the increase in surface-averaged Nusselt number approaches 0 as h/L approaches 0. In general, for all rib heights the highest increase in surface-averaged Nusselt number is observed for either a low rib length or a rib length just below $p/L = 1$. In the limit

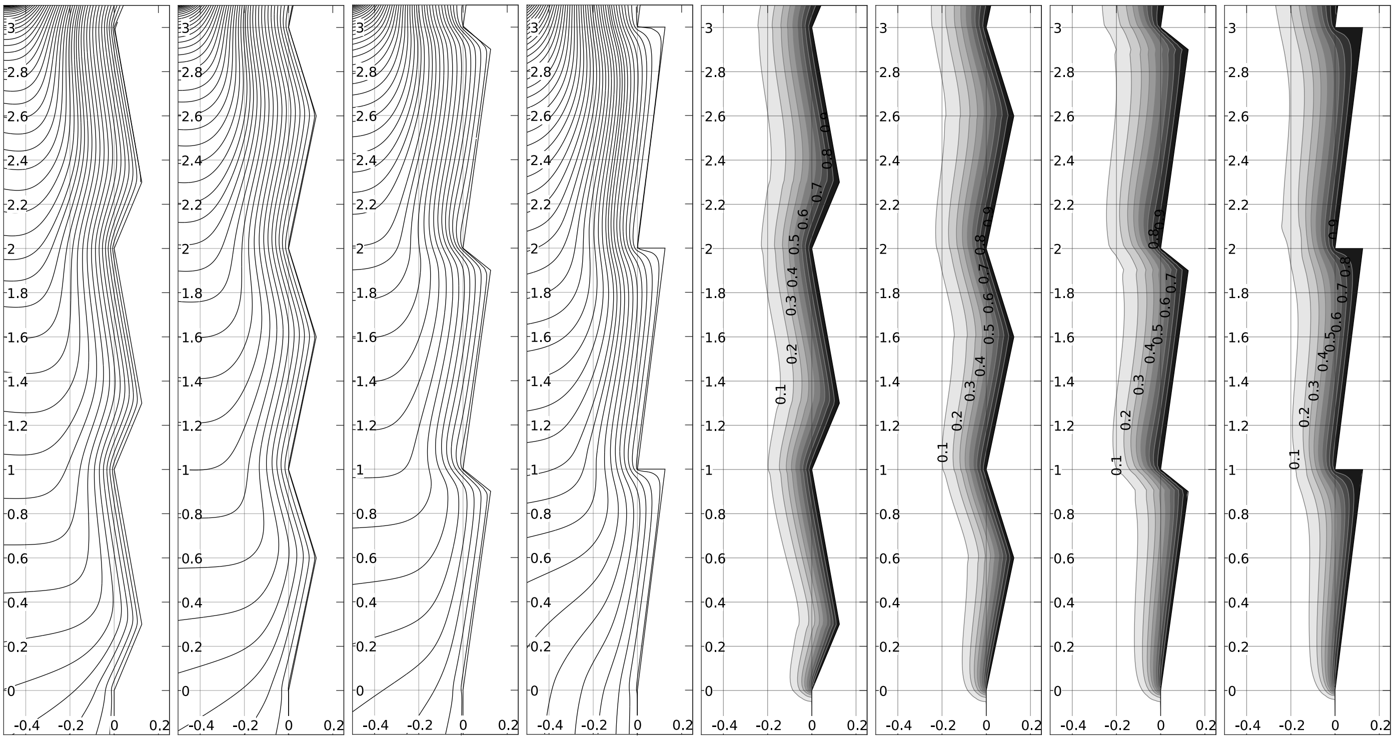

Figure 6: Subfigure 1-4 show streamlines and subfigure 5-8 show the temperature field $\theta = (T - T_\infty)/(T_\mathrm{s} - T_\infty)$ with isotherms for surfaces with $p/L = 0.3$, $p/L = 0.6$, $p/L = 0.9$ and $p/L = 1.0$ for a fixed rib length $h/L = 1/8$, Grashof number $\mathrm{Gr_L} = 10^5$ and Prandtl number $\mathrm{Pr} = 0.71$.

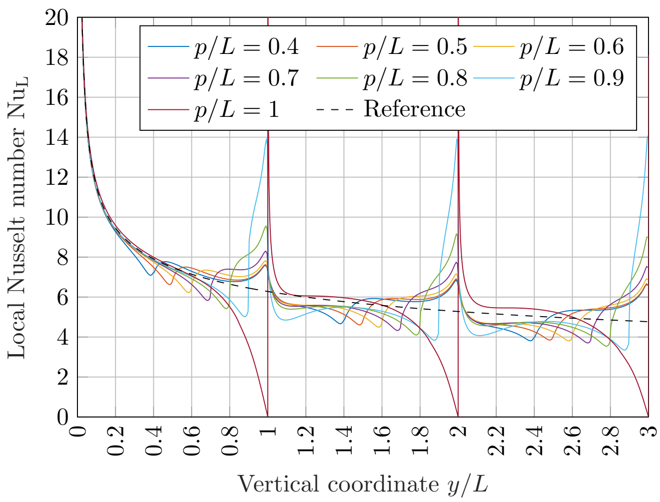

Figure 7: Local Nusselt number $\mathrm{Nu_L}$ as function of vertical distance for various rib lengths at $\mathrm{Gr_L} = 10^5$, $\mathrm{Pr} = 0.71$ and at a fixed rib height $h/L = 1/8$.

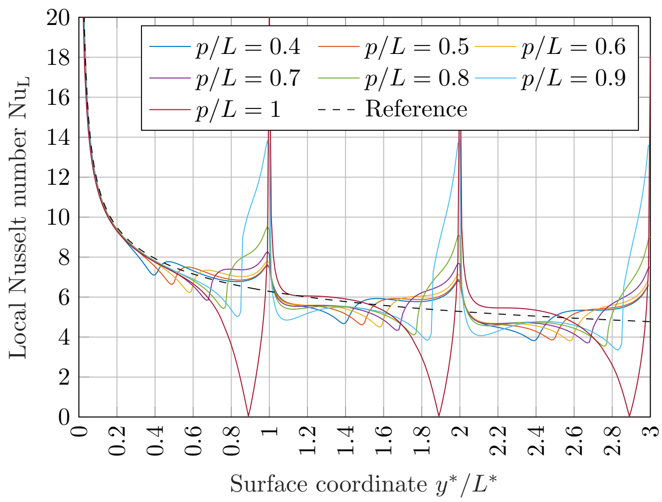

Figure 8: Local Nusselt number $\mathrm{Nu_L}$ as function of local coordinate along the wall (see figure 2) for various rib lengths at $\mathrm{Gr_L} = 10^5$, $\mathrm{Pr} = 0.71$ and at a fixed rib height $h/L = 1/8$.

when $p/L = 1$ a significant drop in surface-averaged Nusselt number is observed. The drop becomes more significant for higher values of rib height and the surface-averaged Nusselt number is decreased compared to the flat vertical surface.

The ribbed surfaces have a higher surface area than the plain surface. Figure 13 shows the relative difference in surface-averaged Nusselt number when the results are scaled according to (11) to account for the difference in surface area. As shown in the figure, the peaks observed at low and high rib heights of $p/L = 0.3$ and $p/L = 0.9$ respectively become even more pronounced when the correction for the increase in surface area is applied. The highest increase in surface-averaged Nusselt number after correcting for the increase in surface area is observed for a surface with a combination of high rib length and height

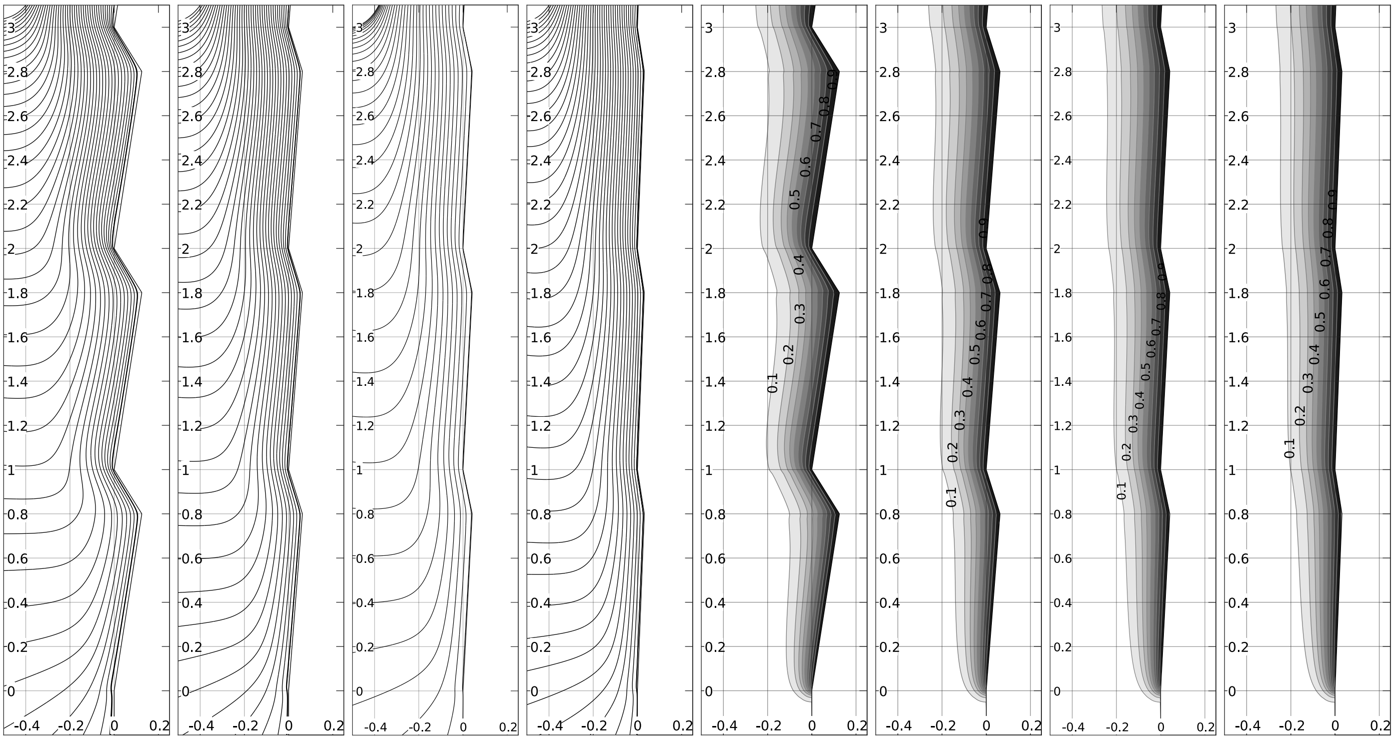

Figure 9: Subfigure 1-4 show streamlines and subfigure 5-8 show the temperature field $\theta = (T - T_\infty)/(T_s - T_\infty)$ and isotherms for surfaces with $h/L = 1/8$, $h/L = 1/16$, $h/L = 1/24$ and $h/L = 1/32$ for a fixed rib length $p/L = 0.8$, Grashof number $\mathrm{Gr_L} = 10^5$ and Prandtl number $\mathrm{Pr} = 0.71$.

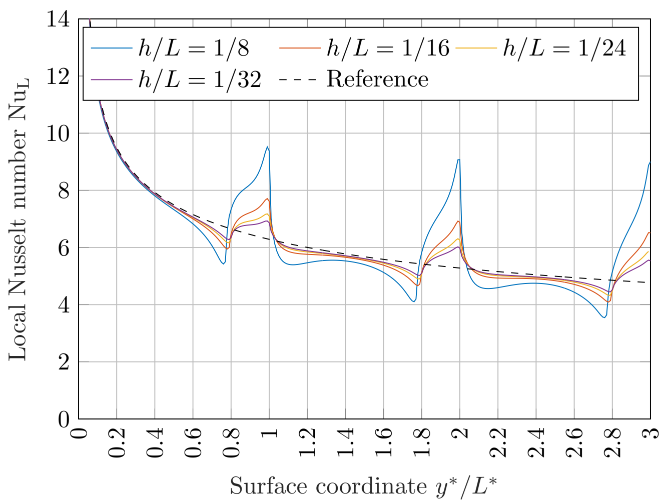

Figure 10: Local Nusselt number $\mathrm{Nu_L}$ for various rib heights at $\mathrm{Gr_L} = 10^5$, $\mathrm{Pr} = 0.71$ and at a fixed rib length $p/L = 0.8$.

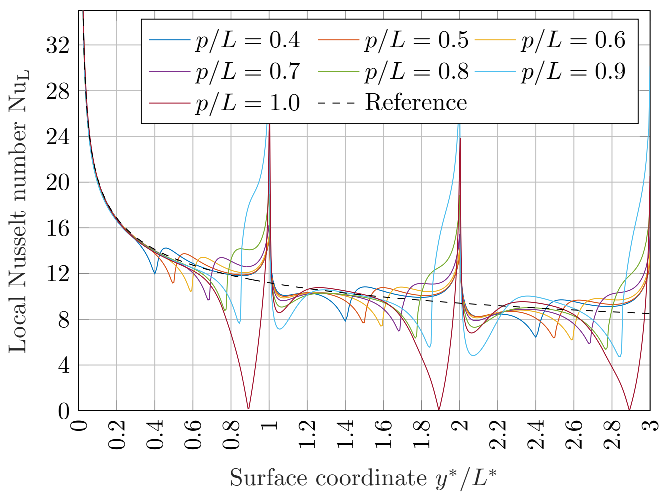

Figure 11: Local Nusselt number $\mathrm{Nu_L} = (\partial T/\partial n)L/(T_s - T_\infty)$ for various rib lengths at $\mathrm{Gr_L} = 10^6$, $\mathrm{Pr} = 0.71$ and at a fixed rib height $h/L = 1/8$.

of $p/L = 0.9$ and $h/L = 1/8$ respectively. Here the zigzag-shaped shaped surface perform 11.60% better than the vertical flat plate. As figure 13 shows, the heat transfer rate is significantly increased just upstream the rib tip.

5. Conclusions

The possibility of enhancing natural convective heat transfer on vertical isothermal surfaces was examined. Unlike previous work dealing mostly with sinusoidal surfaces or square ribs, we introduce zigzag-shaped surfaces to circumvent some of the drawbacks mentioned in previous work. After validating the numerical results obtained in the limiting case of a vertical flat plate, we varied the rib length p/L, rib height h/L for Grashof numbers $\mathrm{Gr_L} = g\beta\,(T_s - T_\infty)\,L^3/\nu^2$ of 10^5 and 10^6 at $\mathrm{Pr} = 0.71$. Summing up, the main findings in this study were:

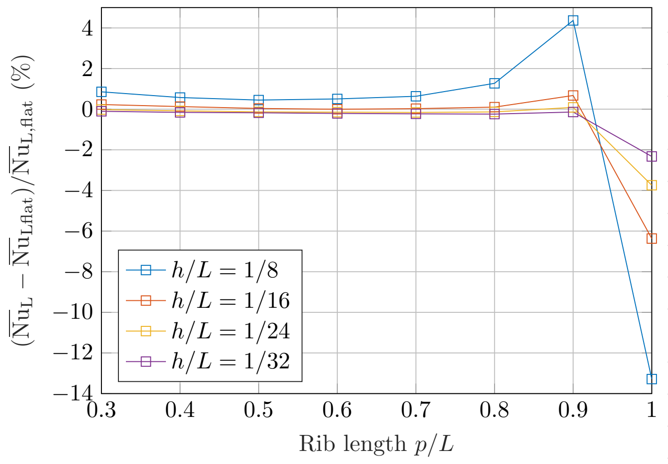

Figure 12: Relative difference in surface-averaged Nusselt number at $\mathrm{Gr_L} = 10^5$ and $\mathrm{Pr} = 0.71$ compared to the flat vertical surface under similar conditions.

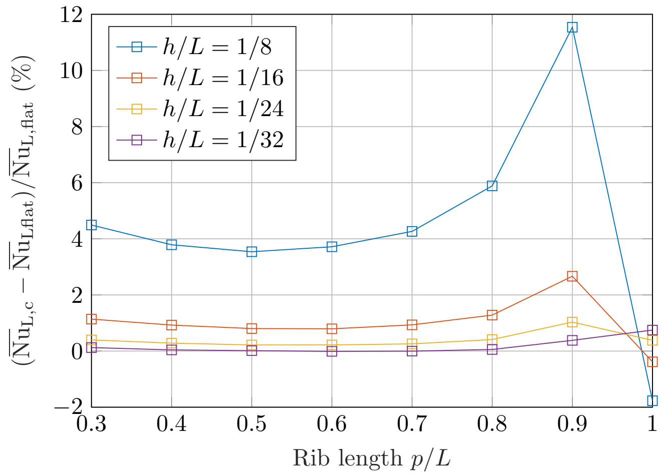

Figure 13: Relative difference in surface-averaged Nusselt number corrected for the increase in surface area for ribbed surfaces at $\mathrm{Gr_L} = 10^5$ and $\mathrm{Pr} = 0.71$ compared to the flat vertical surface under similar conditions. Refer to equation (11) for the correction.

- Natural convective heat transfer may be increased by adding zigzag-shaped ribs to vertical surfaces. For a rib with $p/L = 0.9$ and $h/L = 1/8$ an increase in surface-averaged Nusselt number of 4.43% and 4.94% is observed for $\mathrm{Gr_L} = 10^5$ and $\mathrm{Gr_L} = 10^6$ respectively. These numbers increase to 11.60% and 12.15% when the total heat transfer is considered by correcting for the increase in surface area for the ribbed surfaces.

- The selection of rib length p/L and rib height h/L is critical and if not chosen carefully the zigzag shaped ribs may eventually decrease the overall heat transfer on the surface compared to a plane vertical surface.

- Ribs with horizontal sections (e.g. $p/L = 1$) should be avoided due to the inherent stagnation regions that limit heat transfer in these regions. Instead, horizontal sections should at angled slightly (e.g. $p/L = 0.9$) to circumvent the decrease in local heat transfer in these regions.

- A local peak in surface-averaged Nusselt number is observed for either a low rib length of $p/L = 0.3$ or a high rib length $p/L = 0.9$. The ribs having lengths between $p/L = 0.3$ and $p/L = 0.9$ are shown to perform worse in terms of heat transfer than either limit of $p/L = 0.3$ and $p/L = 0.9$.

- By carefully monitoring local quantities in the present study, no transient phenomena were observed in the flow. Surfaces with slightly higher Grashof number or rib heights are expected to trigger the transition to turbulence.

We suggest future studies on unconfined surface heat transfer enhancement to follow the numerical approach by Faghri and Asakot [27], Kelkar [28] and focus on a periodic section of the geometry. Furthermore, ribs are expected to trigger the transition to turbulence and hence mapping the transition to turbulence for a wide range of geometrical parameters and Grashof numbers is important.

Acknowledgements

This research received no external funding.

References

[1] K. Kalidasan, R. Velkennedy, P. Rajesh Kanna, Buoyancy enhanced natural convection inside the ventilated square enclosure with a partition and an overhanging transverse baffle, International Communications in Heat and Mass Transfer 56 (2014) 121–132, doi:10.1016/j.icheatmasstransfer.2014.06.007.

[2] H. T. Xu, Z. Y. Wang, F. Karimi, M. Yang, Y. W. Zhang, Numerical simulation of double diffusive mixed convection in an open enclosure with different cylinder locations, International Communications in Heat and Mass Transfer 52 (2014) 33–45, doi:10.1016/j.icheatmasstransfer.2014.01.005.

[3] N. Biswas, P. S. Mahapatra, N. K. Manna, Thermal management of heating element in a ventilated enclosure, International Communications in Heat and Mass Transfer 66 (2015) 84–92, doi:10.1016/j.icheatmasstransfer.2015.05.018.

[4] K.-A. Park, A. E. Bergles, Natural Convection Heat Transfer Characteristics of Simulated Microelectronic Chips, Journal of Heat Transfer 109 (1) (1987) 90–96, ISSN 0022-1481, doi: 10.1115/1.3248074.

[5] Y. Joshi, T. Willson, S. J. Hazard III, An Experimental Study of Natural Convection From an Array of Heated Protrusions on a Vertical Surface in Water, Journal of Electronic Packaging 111 (2) (1989) 121–128, doi:10.1115/1.3226516.

[6] S. H. Bhavnani, A. E. Bergles, Effect of surface geometry and orientation on laminar natural convection heat transfer from a vertical flat plate with transverse roughness elements, International Journal of Heat and Mass Transfer 33 (5) (1990) 965–981, doi:10.1016/0017-9310(90)90078-9.

[7] M. Aydin, Dependence of the Natural Convection over a Vertical Flat Plate in the Presence of the Ribs, International Communications in Heat and Mass Transfer 24 (4) (1997) 521–531, doi:10.1016/S0735-1933(97)00037-7.

[8] G. Tanda, Natural convective heat transfer in vertical channels with low-thermal-conductivity ribs, International Journal of Heat and Fluid Flow 29 (5) (2008) 1319–1325, ISSN 0142727X, doi:10.1016/j.ijheatfluidflow.2008.05.004.

[9] G. Tanda, Natural convection heat transfer in vertical channels with and without transverse square ribs, International Journal of Heat and Mass Transfer 40 (9) (1997) 2173–2185, doi: 10.1016/S0017-9310(96)00246-3.

[10] G. Tanda, Experiments on natural convection in water-cooled ribbed channels with different aspect ratios, International Journal of Heat and Mass Transfer 110 (2017) 606–612, ISSN 00179310, doi:10.1016/j.ijheatmasstransfer.2017.03.050, DOI: `http://dx.doi.org/10.1016/j.ijheatmasstransfer.2017.03.050`.

[11] S. Acharya, A. Mehrotra, Natural convection heat transfer in smooth and ribbed vertical channel, International Journal of Heat and Mass Transfer 36 (1) (1993) 236–241, doi: 10.1016/0017-9310(93)80085-9.

[12] L. S. Yao, Natural Convection Along a Vertical Wavy Surface, Journal of Heat Transfer 105 (1983) 465–468, doi: 10.1115/1.3245608.

[13] S. G. Moulic, L. S. Yao, Mixed Convection Along a Wavy Surface, Journal of Heat Transfer 111 (1989) 974–979, doi: 10.1115/1.3250813.

[14] S. G. Moulic, L. S. Yao, Natural Convection Along a Vertical Wavy Surface With Uniform Heat Flux, Journal of Heat Transfer 111 (1989) 1106–1108, doi:10.1115/1.3250780.

[15] M. M. Molla, M. A. Hossain, L. S. Yao, Natural convection flow along a vertical wavy surface with uniform surface temperature in presence of heat generation/absorption, International Journal of Thermal Sciences 43 (2) (2004) 157–163, ISSN 12900729, doi: 10.1016/j.ijthermalsci.2003.04.001.

[16] M. M. Molla, M. A. Hossain, Radiation effect on mixed convection laminar flow along a vertical wavy surface, International Journal of Thermal Sciences 46 (9) (2007) 926–935, ISSN 12900729, doi:10.1016/j.ijthermalsci.2006.10.010.

[17] L.-S. Yao, Natural convection along a vertical complex wavy surface, International Journal of Heat and Mass Transfer 49 (1-2) (2006) 281–286, doi: 10.1016/j.ijheatmasstransfer.2005.06.026.

[18] A. Sharma, P. S. Mahapatra, N. K. Manna, K. Ghosh, P. Wahi, A. Mukhopadhyay, Thermal instability-driven multiple solutions in a grooved channel, Numerical Heat Transfer, Part A: Applications 70 (7) (2016) 776–790, doi: 10.1080/10407782.2016.1192936.

[19] A. Cimarelli, D. Angeli, Routes to chaos of natural convection flows in vertical channels, International Communications in Heat and Mass Transfer 81 (2017) 201–209, ISSN 07351933, doi:10.1016/j.icheatmasstransfer.2016.12.025, DOI: `http://dx.doi.org/10.1016/j.icheatmasstransfer.2016.12.025`.

[20] M. Qiao, Z. F. Tian, Q. Yang, X. Feng, Transition to chaos for buoyant flows in a groove heated from below, Physics of Fluids 32 (5) (2020) 054104, doi:10.1063/5.0004288.

[21] S. H. Bhavnani, A. E. Bergles, Natural convection heat transfer from sinusoidal wavy surfaces, Wärme- und Stoffübertragung 26 (6) (1991) 341–349, doi:10.1007/BF01591667.

[22] J. Hærvig, A. L. Jensen, H. Sørensen, Can natural convection on smooth vertical plates in the laminar regime be improved by adding forward facing triangular elements?, in: Proceedings of the ASME - JSME - KSME Joint Fluids Engineering Conference 2019, 1–7, 2019.

[23] R. I. Issa, Solution of the implicitly discretised fluid flow equations by operator-splitting, Journal of Computational Physics 62 (1) (1986) 40–65, doi:10.1016/0021-9991(86)90099-9.

[24] S. Ostrach, An Analysis of Laminar Free-Convection Flow and Heat Transfer about a Flat Plate Parallel to the Direction of the Generating Body Force, Tech. Rep., Lewis Flight Propulsion Laboratory, Cleveland,Ohio, 1952.

[25] E. J. L. Fevre, Laminar free convection from a vertical plane surface, in: 9th International Congress for Applied Mechanics (2nd. Ed.), 168–174, 1956.

[26] P. Roache, Perspective: A Method for Uniform Reporting of Grid Refinement Studies, Journal of Fluids Engineering 116 (3) (1994) 405–413, doi:10.1115/1.2910291.

[27] M. Faghri, Y. Asakot, Periodic, fully developed, natural convection in a channel with corrugated confining walls, International Journal of Heat and Mass Transfer 29 (12) (1986) 1931–1936, ISSN 00179310, doi:10.1016/0017-9310(86)90011-6.

[28] K. M. Kelkar, Numerical prediction of periodically fully developed natural convection in a vertical channel with surface mounted heat generating blocks, International Journal of Heat and Mass Transfer 36 (5) (1993) 1133–1145, doi:10.1016/S0017-9310(05)80084-5.

Nomenclature

A	Actual surface area	L^2
A_p	Projected surface area	L^2
$\boldsymbol{g}$	Gravitational acceleration	$\mathrm{L}\ \mathrm{T}^-2$
Gr_L	Local Grashof number	1
h	Rib height (see figure 2)	L
L	Pitch distance (see figure 2)	L
L^*	Pitch distance along surface	L
$\boldsymbol{n}$	Wall normal unit vector (see figure 2)	1
Nu_L	Local Nusselt	1
p	Rib length (see figure 2)	L
Pr	Prandtl number	1
t	Time	T
t^*	Dimensionless time	1
T	Temperature	θ
T_s	Surface temperature	θ
T_∞	Temperature unaffected by surface	θ
$\boldsymbol{u}$	Velocity vector	$\mathrm{L}\ \mathrm{T}^{-1}$
x, y	Global coordinate system	L
y^*	Local coordinate along the surface	L
α	Thermal diffusivity	$\mathrm{L}^2\ \mathrm{T}^{-1}$
β	Coefficient of volumetric expansion	θ^{-1}
ν	Kinematic viscosity	$\mathrm{L}^2\ \mathrm{T}^{-1}$
θ	Dimensionless temperature	1
Notation		
$\overline{x}$	Surface averaging, $\overline{x} = A^{-1}\int_A x\ \mathrm{d}A$	
x_c	Surface area correction using A/A_p	

Appendix A. Tabulated Data

Table A.1: Surface-averaged Nusselt numbers $\overline{\mathrm{Nu}}_{\mathrm{L}}$, the relative difference from the flat surface and the relative difference from the flat surface corrected for the area ratio. Refer to equation (11) for the surface area corrected Nusselt number $\overline{\mathrm{Nu}}_{\mathrm{L,c}}$.

h/L	p/L	Pr	$\overline{\mathrm{Nu}}_{\mathrm{L}}$		$(\overline{\mathrm{Nu}}_{\mathrm{L}} - \overline{\mathrm{Nu}}_{\mathrm{Lflat}})/\overline{\mathrm{Nu}}_{\mathrm{L,flat}}$ (%)		$(\overline{\mathrm{Nu}}_{\mathrm{L,c}} - \overline{\mathrm{Nu}}_{\mathrm{Lflat}})/\overline{\mathrm{Nu}}_{\mathrm{L,flat}}$ (%)	
			$\mathrm{Gr_L} = 10^5$	$\mathrm{Gr_L} = 10^6$	$\mathrm{Gr_L} = 10^5$	$\mathrm{Gr_L} = 10^6$	$\mathrm{Gr_L} = 10^5$	$\mathrm{Gr_L} = 10^6$
0 (flat surface)	-	0.71	6.505	11.476	1.00	1.00	1.00	1.00
1/8	0.3	0.71	6.561	11.604	0.85	1.11	4.49	4.75
1/16	0.3	0.71	6.520	11.534	0.23	0.50	1.14	1.41
1/24	0.3	0.71	6.504	11.508	-0.02	0.28	0.40	0.70
1/32	0.3	0.71	6.498	11.499	-0.01	0.19	0.12	0.42
1/8	0.4	0.71	6.542	11.580	0.57	0.90	3.79	4.13
1/16	0.4	0.71	6.514	11.522	0.13	0.40	0.93	1.20
1/24	0.4	0.71	6.500	11.502	-0.08	0.23	0.28	0.59
1/32	0.4	0.71	6.495	11.493	-0.16	0.15	0.04	0.35
1/8	0.5	0.71	6.534	11.579	0.45	0.85	3.54	3.95
1/16	0.5	0.71	6.508	11.517	0.04	0.35	0.80	1.12
1/24	0.5	0.71	6.497	11.501	-0.13	0.20	0.22	0.55
1/32	0.5	0.71	6.494	11.493	-0.18	0.14	0.01	0.33
1/8	0.6	0.71	6.538	11.602	0.50	0.89	3.72	4.12
1/16	0.6	0.71	6.505	11.521	0.00	0.36	0.79	1.16
1/24	0.6	0.71	6.496	11.499	-0.15	0.21	0.22	0.58
1/32	0.6	0.71	6.492	11.493	-0.21	0.14	-0.01	0.34
1/8	0.7	0.71	6.546	11.602	0.63	1.09	4.26	4.74
1/16	0.7	0.71	6.507	11.521	0.03	0.39	0.93	1.30
1/24	0.7	0.71	6.495	11.499	-0.16	0.20	0.26	0.62
1/32	0.7	0.71	6.490	11.493	-0.23	0.14	0.00	0.37
1/8	0.8	0.71	6.588	11.674	1.27	1.72	5.89	6.35
1/16	0.8	0.71	6.512	11.534	0.10	0.50	1.28	1.69
1/24	0.8	0.71	6.496	11.507	-0.13	0.27	0.41	0.81
1/32	0.8	0.71	6.489	11.494	-0.24	0.15	0.06	0.45
1/8	0.9	0.71	6.793	12.044	4.43	4.94	11.60	12.15
1/16	0.9	0.71	6.549	11.609	0.67	1.16	2.67	3.16
1/24	0.9	0.71	6.511	11.532	0.09	0.48	1.03	1.43
1/32	0.9	0.71	6.496	11.506	-0.14	0.26	0.38	0.78
1/8	1.0	0.71	5.641	9.926	-13.28	-13.51	-1.77	-2.03
1/16	1.0	0.71	6.091	10.662	-6.37	-7.10	-0.38	-1.16
1/24	1.0	0.71	6.262	10.981	-3.74	-4.32	0.38	-0.22
1/32	1.0	0.71	6.354	11.167	-2.33	-2.69	0.75	0.37